REGULAR PAPER

Condition Assessment of Low Voltage Photovoltaic DC Cables under Thermal Stress Using Non-Destructive Electrical Techniques

Ehtasham Mustafa[1] · Ramy S. A. Afia[1,2] · Zoltán Ádám Tamus[1]

Abstract

The output power of the photovoltaic system is heavily dependent on the low voltage (LV) DC cables which are exposed to multiple stresses such as climatic, mechanical, electrical, and thermal stress, hence makes them more exposed to aging as compared to other components in the system. Accordingly, it is essential to monitor the state and know the real cause of the insulation degradation of the cable. The physio-chemical changes inside the insulation during service is attributed to the thermal stress, which the cable has to endure constantly. Traditionally, destructive test techniques have been adopted to study the aging phenomenon in the cable insulation, making them unsuitable for on-line condition monitoring. This research work has been aimed to study the degradation in LV photovoltaic DC cables under thermal stress by measuring the dielectric properties; complex permittivity, tanδ with the change in frequency and decay and return voltage slopes using extended voltage response method. The non-destructive diagnostic methods used are based on the phenomenon of polarization and conduction in the insulation material. The noteworthy change in the values of the imaginary part of permittivity, tanδ at low frequencies, and the overall decrease in the values of return voltage slope showed the change in the structure of the polymer matrix under the stress which was related to the cross-linking based chemical reactions. The results show that the techniques can be adopted for the on-line condition monitoring of the cable for the PV system and the dielectric parameters can be used to study the chemical and physical changes happening inside the material effectively.

Keywords Photovoltaic power system · Low voltage DC cables · Thermal stress · Complex permittivity · Extended voltage response

1 Introduction

The share of renewable energy in the over-all world electricity consumption is rapidly growing due to its clean, green and reusable characteristics [1]. The photovoltaic (PV) system is one such renewable energy source out of other available sources which has been recognized as a cost-competitive, safe, environment-friendly, and reliable source of energy. It has been predicted that PV will surpass its competitor wind in new installed capacity in the coming years as a result of huge price declines in recent times [2–4]. With more PV installation and usage, the knowledge and experience with this system have also increased [5]. This results in the observation and reporting of such faults which occur very occasionally, one such rare case is the failure of DC cable insulation [6].

In a PV system the four main components are to be connected, PV modules, the charge controller, the batteries and the inverter [4]. DC cables are used to connect the PV module and the inverter; converts the DC power into AC power which is the most important one and as the most popular form of electricity accepted in appliances. Although the DC cables account for only 2% in the solar project cost but they have a significant impact on the power output [7]. The PV modules and the DC cables are vulnerable to several extreme environmental conditions such as hot and cold temperatures, humidity, UV radiation, and wind [8]. In addition to the environmental stress, the DC cables also have to bear the mechanical and electrical stresses such as bending and

✉ Ehtasham Mustafa
  mustafa.ehtasham@vet.bme.hu

1 Department of Electric Power Engineering, Budapest University of Technology & Economics, 18 Egry Joszef Street, 1111 Budapest, Hungary

2 Department of Electrical Power and Machines Engineering, Helwan University, 1 Sherif Street, Helwan, Cairo 11792, Egypt

voltage drop heating, respectively. Since the insulation of the cables is a polymer in nature, so the temperature stress and the voltage drop heating; combined as thermal stress affects the structure of the polymer [9, 10]. This degradation phenomenon in cables is of more concerned than in other components of the PV systems as the thermal stress creates a chemical and physical alteration in the properties of the insulation. This may lead to safety hazards and reduced power output, in addition to the generation of leakage current which could end up in insulation failure and hence system failure. The cost of system shutdown combined with the cable replacement and repair is very high. Hence, this makes necessary to have the knowledge of the state and properties of the cable insulation and the mechanism of failure during operation. In this scenario, using the type of diagnostic method to study the cable insulation is imperative.

The change in the structure of the insulation material due to thermal stress results in a change in the chemical, mechanical and electrical characteristics of the material [11]. One way to study these changes happening inside the material is to use destructive chemical methods; density, ultrasonic velocity, thermogravimetric analysis (TGA), gel content, Fourier-transform infrared spectroscopy (FTIR), and oxidation induction time (OIT), and mechanical methods; elongation at break (EaB) and indenter modulus (IM) [12]. Due to destructive nature of the tests, their application for on-line condition monitoring has been limited. Since the primary purpose of the electrical insulation is its electrical integrity, so it is important to study the dielectric characteristics. The study of conduction and polarization phenomenon in the material is one such method that helps in understanding the changes happening inside the insulation material due to the thermal stress.

Cross-linked polyolefin (XLPO) has been widely used polymer in PV insulation DC cables due to a number of advantages such as thermal stability, dielectric properties, and solvent resistance. But XLPO has shown anomalous behavior during aging and has been reported in a number of literature [13–15]. The behavior of XLPO has been studied in these literature using destructive chemical and mechanical techniques. In this paper, the conduction and polarization phenomenon has been studied in view of the electrical properties of the complex permittivity (ε^*), dissipation factor (tanδ), decay voltage slope (S_d) and return voltage slope (S_r), being non-destructive methods. The phenomenon has been studied using component analyzer and extended voltage response (EVR) methods for thermally aged low voltage (LV) PV DC cables. Although a number of researchers have studied the electrical properties due to aging in LV cables [16–19] but none of them have studied the phenomenon for PV DC cables, which need due consideration for the safe and reliable operation of PV system. The prominent change in the values of tanδ, the imaginary part of permittivity (ε^ε) and return voltage slopes (S_r) proved that the applied methods are reliable and effective in studying the aging phenomenon in the PV DC cables without any damage to the cables, making them suitable for the on-line condition monitoring adopted for the PV system.

The paper has been organized as follows: the cable structure and characteristics, accelerated thermal aging, measurement of dielectric properties and EVR setup have been presented in Sect. 2. In Sect. 3, the results of the measurements have been laid out and a discussion on them in Sect. 4. While the conclusion and further prospects have been discussed in Sect. 5.

2 Experimental Work

2.1 Materials

The LV PV DC cable under investigation had the inner insulation and jacket composed of XLPO, Fig. 1a. The cable had a single-stranded copper conductor with tin plating

Fig. 1 **a** Low voltage power cable sample under investigation; **b** Air circulating oven for thermal aging

(a)

(b)

(diameter = 2.25 mm). The outer diameter of the cable was 5.8 mm. A short length of the insulation was removed from the conductor and a short length of the jacket was removed from the insulation to prevent any leakage current to flow during measurements.

2.2 Accelerated Aging

The cable samples under consideration, one meter long were subjected to thermal stress at 120 °C for four cycles; 240, 480, 720 and 960 h in an air circulating oven, Fig. 1b. The thermal cycles were equivalent to 20, 40, 60 and 80 years of service time at 60 °C, which were based on the calculation using Arrhenius's relationship with taking the activation energy of 1.24 eV into account. The jacket and the insulation were kept in contact with the conductor to obtain the results as the cable is subjected to the field conditions. After each thermal cycle, the samples were removed from the oven for analysis.

2.3 Measurement of Dielectric Properties

Precision Component Analyzer was used to study the dielectric properties, real (ε') and imaginary (ε'') part of complex permittivity and dielectric loss (tanδ). The impedance and tanδ of the cable samples were measured with an R–C parallel configuration setup for a frequency range of 20 Hz to 500 kHz at an applied voltage of 5 V_{rms} and at a room temperature of 25 °C ± 2%. The input signal was applied to the conductor and the output signal was measured from a wire braid positioned on the outer surface of the cable. The cable samples and the electrodes were placed in the Faraday cage to reduce any pickup from the external noises.

The real permittivity (ε') is a measure of how the external field energy is amassed within a material while how the material dissipates the energy from the external field is defined by the imaginary part of permittivity (ε'') [20–23]. The real and imaginary part of the complex permittivity were evaluated from the measured data using the expressions [24]:

$$\varepsilon' = \frac{C(\omega)}{C_o} \tag{1}$$

$$\varepsilon'' = \frac{1}{2\pi f R C_o} \tag{2}$$

where C_o is the reference capacitance and is calculated by the known dimensions of the cable and the electrodes, while f being the particular frequency during measurement.

The tanδ is defined as the ratio of the imaginary part of permittivity (ε'') to the real part of permittivity ε'. Whenever a dielectric is subjected to an electric field, there are a number of losses; conduction, polarization, and partial discharge losses [25]. The first two losses are developed at a low electric field while the partial discharge losses happen at a high electric field. The conduction phenomenon is due to the transportation of the mobile charge carriers while the polarization is a complex phenomenon, which results due to several elementary processes. The measurement of tanδ at the low electric field, as in our case, is very effective in studying the phenomenon of conduction and polarization in the material.

2.4 Extended Voltage Response

Whenever a structural change happens in the polymer matrix due to aging, it alters the dielectric property of the material. This change can be detected by studying the dielectric polarization phenomenon inside the material by applying a number of techniques classified based on frequency-domain and time-domain methods. One such time-domain method is the Extended Voltage Response (EVR) method. The method is very effective for studying those dielectric polarization processes which have high relaxation time constant or happening at a very low frequency such as the bulk, interfacial and hopping polarization processes. The EVR method is an extended version of the voltage response method and in recent times it has been implemented successfully to study the phenomenon in LV cables used in nuclear power plants, distribution systems and in high voltage cables and transformer insulations [26–30].

The basic working operation of the EVR measurement is shown in Fig. 2a. The insulation material is first charged at a DC voltage of 1000 V for 4000 s. After the charging period, the material is discharged for 20 discharging periods i.e., from 1 to 2000s, which gives a wide range of slow polarization spectrum, Fig. 2b. From the method two voltage slopes; decay (S_d) and return (S_r) voltage slopes are measured, which is calculated by the two equations [31]:

$$S_d = \left(V_{ch}/\in_\infty\right)\gamma \tag{3}$$

$$S_r = \left(V_{ch}/\in_\infty\right)\beta \tag{4}$$

The decay voltage slope (S_d) is generated when the charges on the electrodes are discharged in the insulation after the separation of the insulation from the voltage source and is directly related to the specific conductivity (γ) of the insulation. While the return voltage slope (S_r) is related to the polarization conductivity (β) and is produced after a short discharging period, as a result, the polarization processes which remained excited in the insulation start to relax.

For the LV PV DC cable, the voltage was applied between the conductor and the outer surface of the cable, Fig. 3. All the measurements were carried out at a temperature of 25
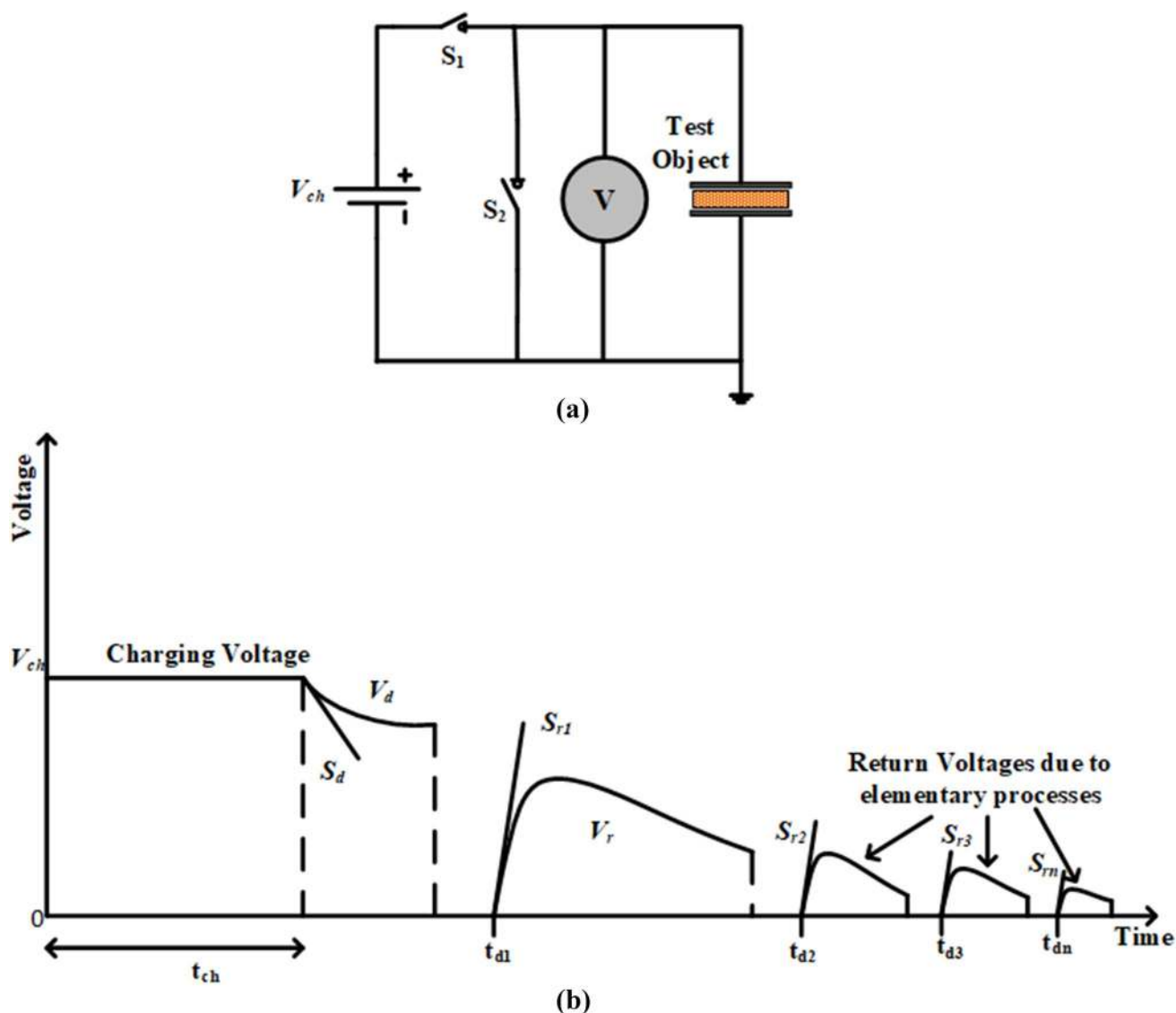
Fig. 2 Extended voltage response **a** Circuit; **b** Timing diagram

°C $\pm 2\%$ and humidity of $25\% \pm 2\%$. After the EVR measurements, the cable samples were discharged for 5 h before the start of the next thermal cycle.

3 Measurement Results

3.1 Dielectric Properties of Unaged and Aged Cable Samples

Figure 4 shows the ε' of the unaged and aged cable samples. Irrespective of the aging, the ε' of the cable increased as the values of the frequency were shifted to lower values. The ε' decreased after the first thermal cycle at all frequencies. While an increase in the values of ε' was observed after the

next three thermal cycles for the whole frequency range and became closer to the values of the unaged ones.

Figure 5a shows the ε'' of the PV cable for the range of frequency under consideration. The ε'' started from a higher value at high frequency and then moved to a minimum value with a decrease in the frequency. This behavior had been observed for both unaged and aged cable samples. The ε'' showed an interesting character with the change of frequency due to aging. After the first thermal cycle, a decreased in the values of ε'' was noted. An increase in the values of ε'' was observed between a frequency range of 200 Hz and 20 kHz after the second thermal cycle. While at all other frequencies a decrease was detected. After the third thermal cycle, a decrease in the values of ε'' was noted at the frequency ranges of 20 to 200 Hz and 800 Hz to 5 kHz, whereas at all

Fig. 3 Measurement setup of extended voltage response
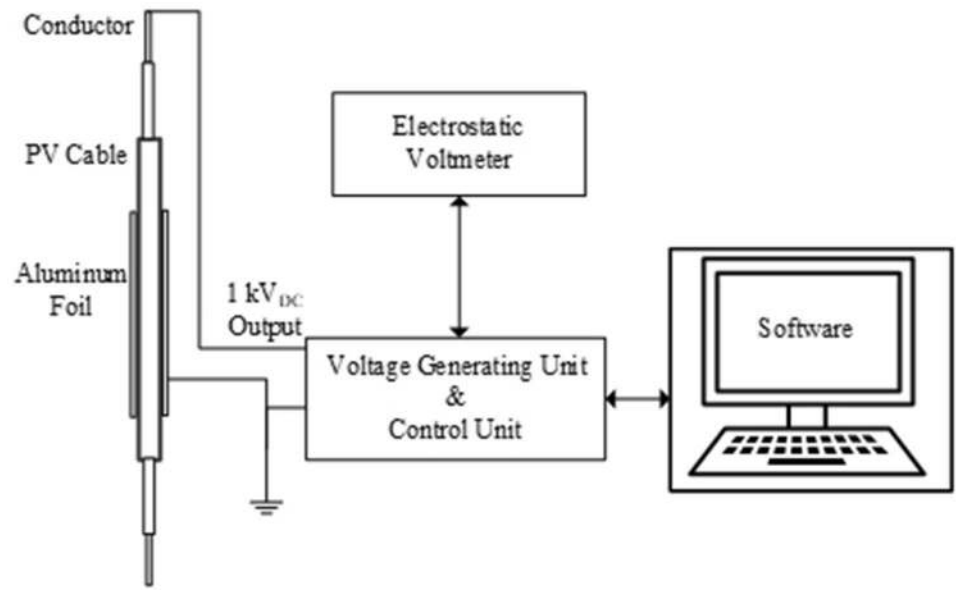
**Fig. 4** Relative permittivity (ε') vs. Frequency for different aging times
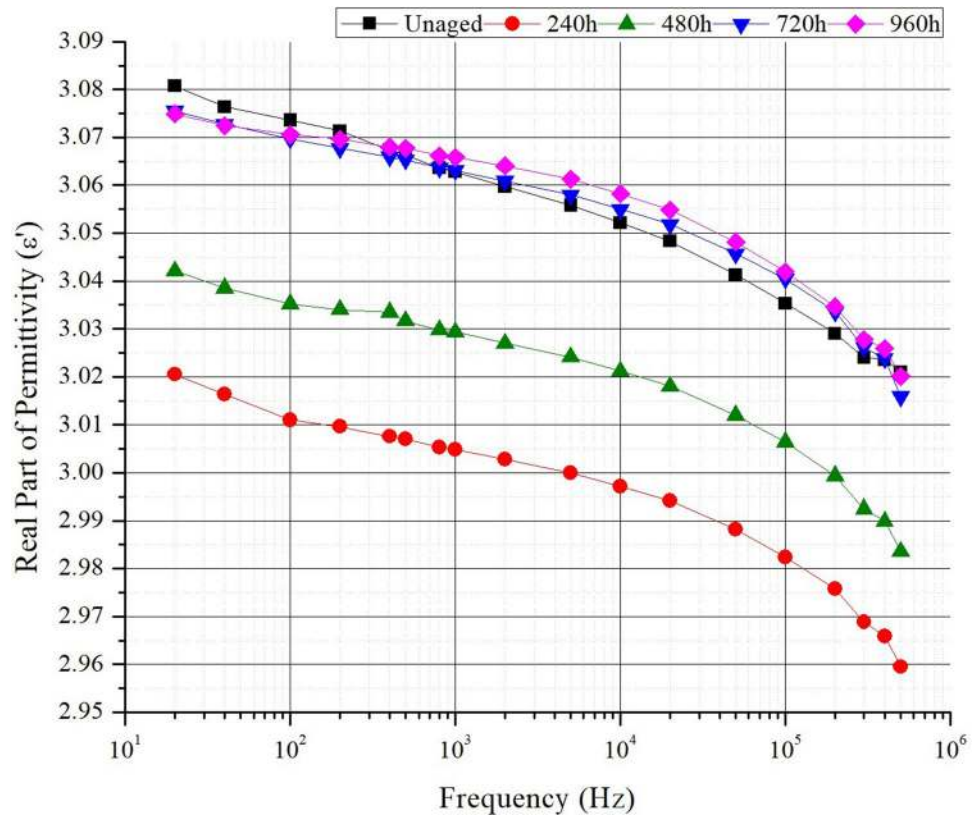
other frequencies, an increase was observed. At the end of the fourth thermal cycle, there was an increase between 5 and 500 kHz, though a decrease was observed between 20 Hz and 2 kHz in the ε''.

For the briefness, four reference frequencies had been selected; 100 Hz, 200 Hz, 10 kHz, and 200 kHz, and plotted against the equivalent aging time in years, Fig. 5b. As can be

observed that the ε'' values had decreased at low frequencies, i.e., 100 Hz and 200 Hz as compared to high frequencies.

The tanδ of the unaged and aged cable is shown in Fig. 6a. There was a decrease of tanδ as the frequency was decreased, starting from a maximum value and after reaching a minimum value at a certain frequency, there was an increase again in the tanδ. This variation of the tanδ with
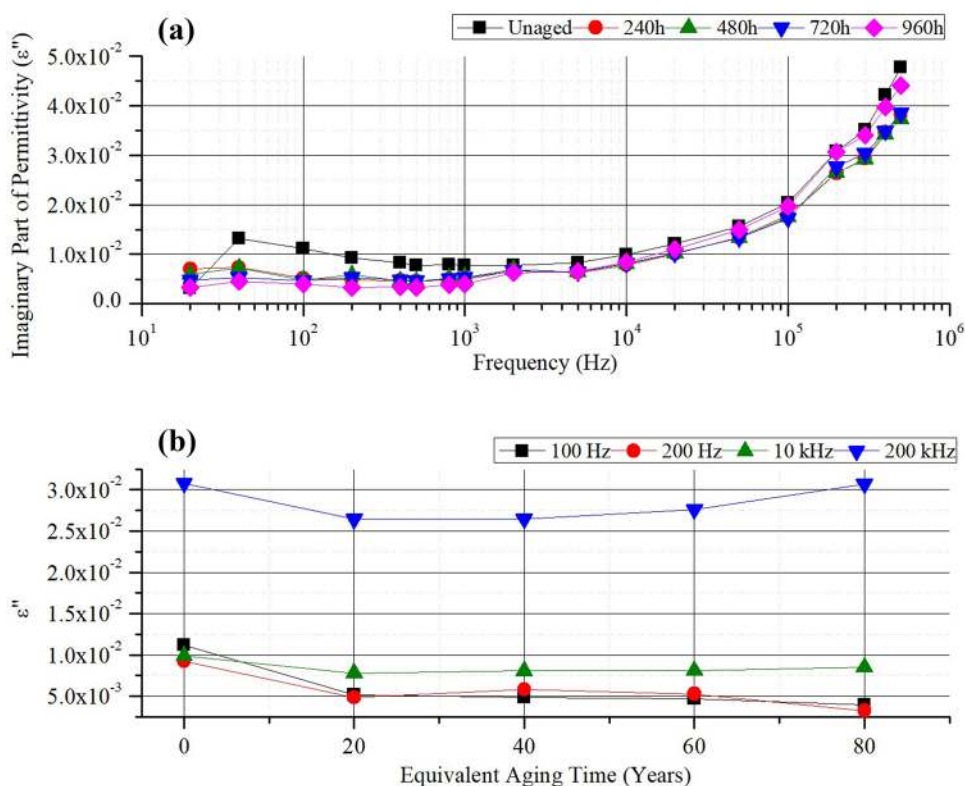
frequency was also irrespective of the aging cycle. Similar to ε'', the effect of aging on the tanδ values was also very interesting. After the first thermal cycle, there was an overall decrease in the tanδ for the whole range of frequency. While, after the second thermal cycle, at the frequency range of 500 Hz to 20 kHz, there was an increase in the values of tanδ. Whereas for a range of 20 to 400 Hz and 50 kHz to 500 kHz there was a decrease in the values. After the third and the fourth thermal cycle, a decrease in the values of tanδ had been observed for the frequency range of 20 Hz to 100 kHz and 20 Hz to 5 kHz, respectively. Even though an increase in the values had been observed between 200 and 500 kHz for the third and between 5 and 500 kHz for the fourth thermal cycles. Figure 6b reports the tanδ at four reference frequencies; 100 Hz, 200 Hz, 10 kHz, and 200 kHz against equivalent aging time, where a decrease in the values at low frequencies was noted with aging.

3.2 EVR Measurements

The results of the EVR are shown in Fig. 7a and b for S_d and S_r respectively. The values of S_d increased after the first and second thermal cycle. While a decrease was observed after the third thermal cycle and then an increase after the fourth thermal cycle. The overall effect was an increase in the values of S_d. The S_r for the different aging cycles are plotted against the discharging time. It was observed that with the increase of the thermal stress, the S_r increased after

the first and second thermal cycle. But after the third and the fourth thermal cycle, a decrease in the values of the S_r had been observed. Overall, the effect of thermal stress was an increase in the values of S_r in reference to the unaged sample values.

4 Discussion

4.1 Dielectric Properties

The polarization phenomenon inside the material has a strong relationship with the ε' [32]. Since there was no discrepancy in relation to the frequency for the ε' of unaged and aged samples, so the ε' is independent of the frequency. The initial decrease in the ε' is due to the creation of the space charges, as it decreases the value of the permittivity. The increase of the permittivity after each thermal cycle shows that the dipolar by-products have been created which are adding to the polarization of the material. This shows that the structural changes happen inside the material.

The results of the ε'' show the dependency of ε'' on the frequency. The change in the values of the ε'' with aging was more prominent at a low frequency than at the high frequencies, which depicts that at higher frequencies the dependence of ε'' on aging is almost insignificant, Fig. 8. The greater change of ε'' at the low frequency shows that due to the thermal stress there has been a strong effect on the polymer
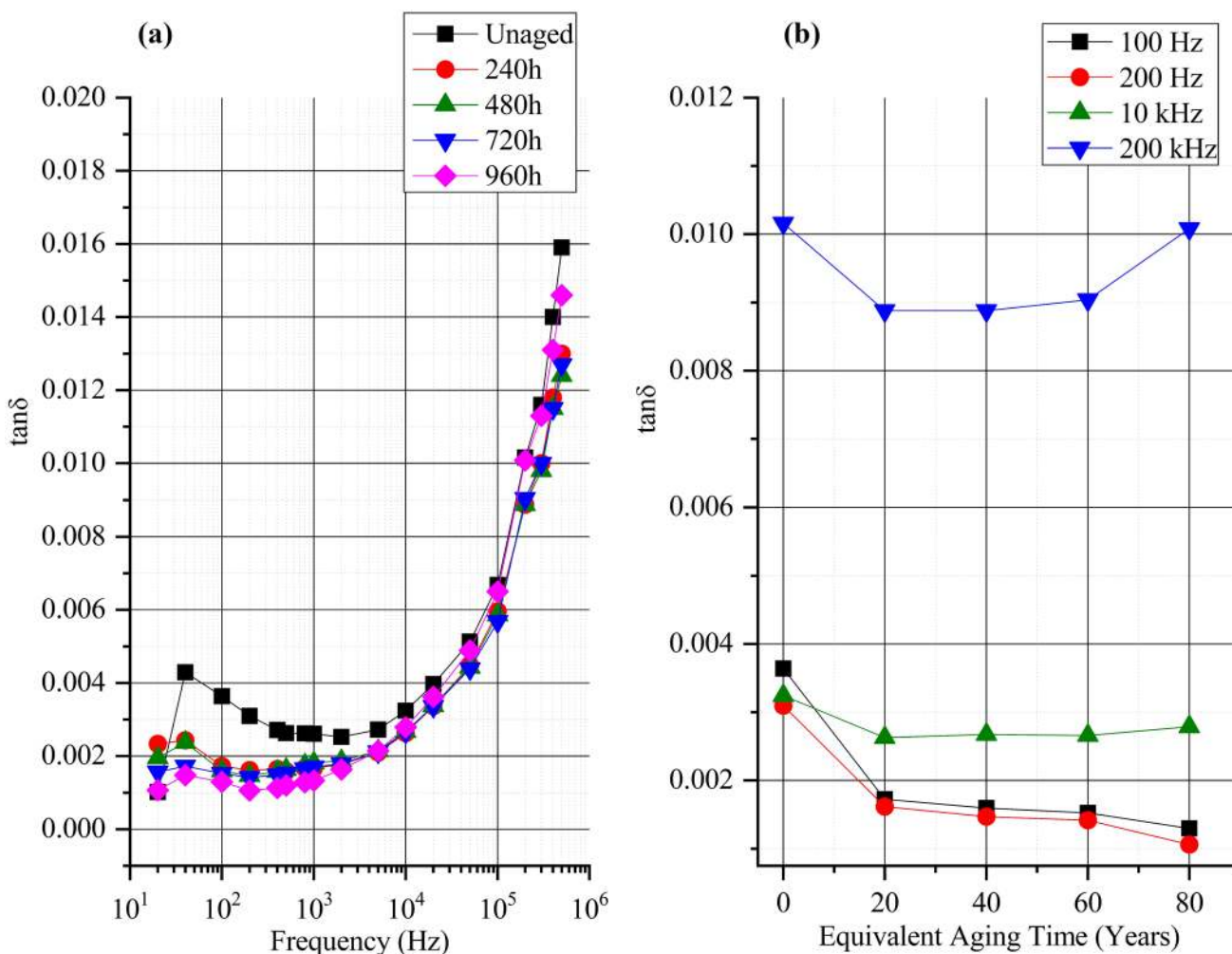
Fig. 6 **a** tanδ vs. Frequency with different aging time; **b** tanδ vs. Equivalent Aging Time (Years) at 100 Hz, 200 Hz, 10 kHz, and 200 kHz

matrix. The creation of new bonds with a reduction of charge carriers is increasing with the thermal stress, as the change in the values of ε'' is increasing with each thermal cycle at the low frequency.

Since the tanδ is considered to be composed of three main losses; conduction, polarization, and partial discharge losses. The variation of the tanδ values is also quite large at the lower frequency than to the higher one, Fig. 9. The tanδ values decreased with the aging cycle at a lower frequency, showing that the losses due to polarization and conduction charge particles have decreased with aging. This suggests the formation of cross-linking based chemical reactions, which is a three-dimensional network within the molecules and restricts the mobility of charge transportation. The values of tanδ at different aging times with reference to values of unaged have been plotted, Fig. 9, against different aging times at three different frequencies, 100 Hz, 200 Hz, and 400 Hz, which clearly shows how the charge mobility has decreased with aging. The high change in the values of ε''

and tanδ shows that the phenomenon contributing to the alteration to the dielectric property of the insulation material has reached to either conclusion or stabilization after 40–80 years.

4.2 EVR

As discussed for the dielectric properties results, the cross-linking reactions due to excessive thermal stress also results in the decrease of the interfacial polarization. The cross-linking reaction not only limits the charge movement but also restricts the dipole orientation, hence results in the decrease of polarization. This phenomenon has been associated with XLPO, as at elevated temperature the cross-linking occurs, which creates a kind of repair mechanism [10, 13, 14].

The increase in the S_d values shows the increase in the specific conductivity of the material. The structural changes happening inside the material due to the thermal stress results in the production of localized sites for

Fig. 7 EVR Measurements **a** S_d vs. Aging time; **b** S_r vs. Discharging time for different aging times
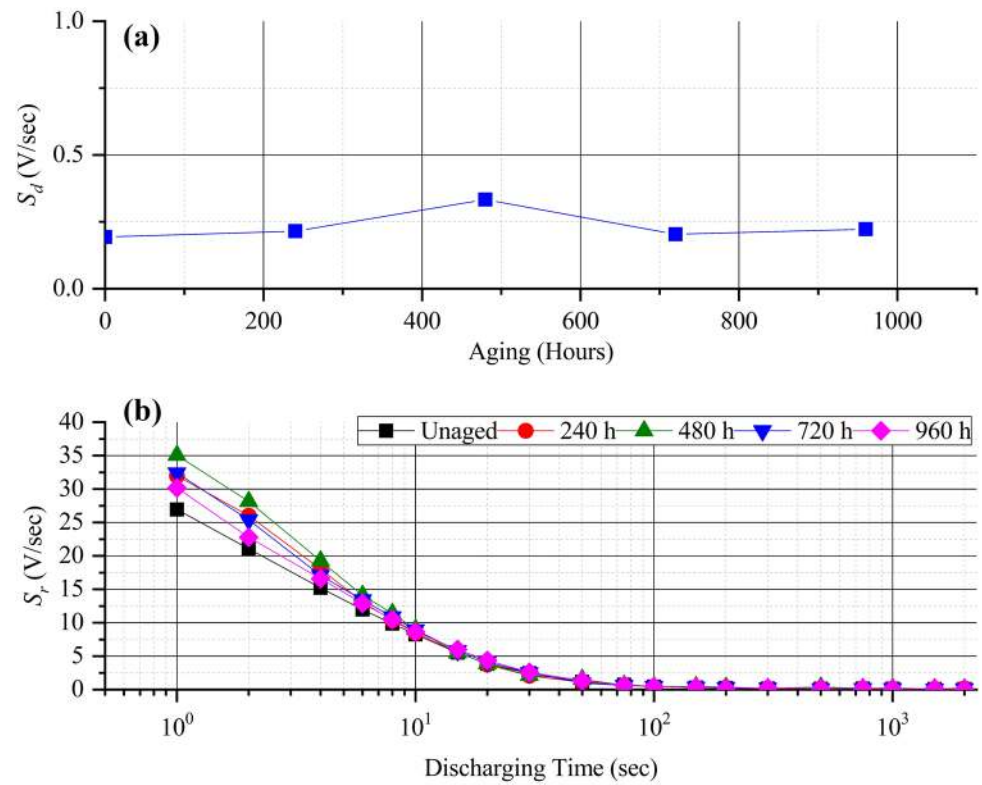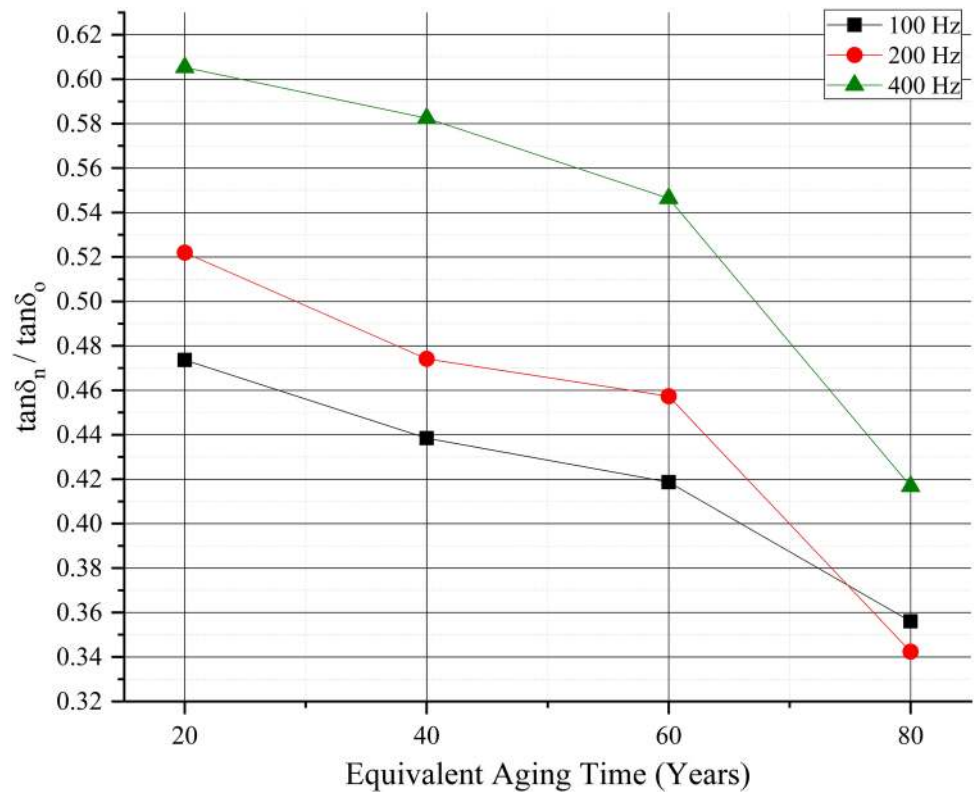

Fig. 8 The behavior of the imaginary part of permittivity at 100 Hz, 10 kHz, and 200 kHz with reference to unaged values against Equivalent Aging Time in Years
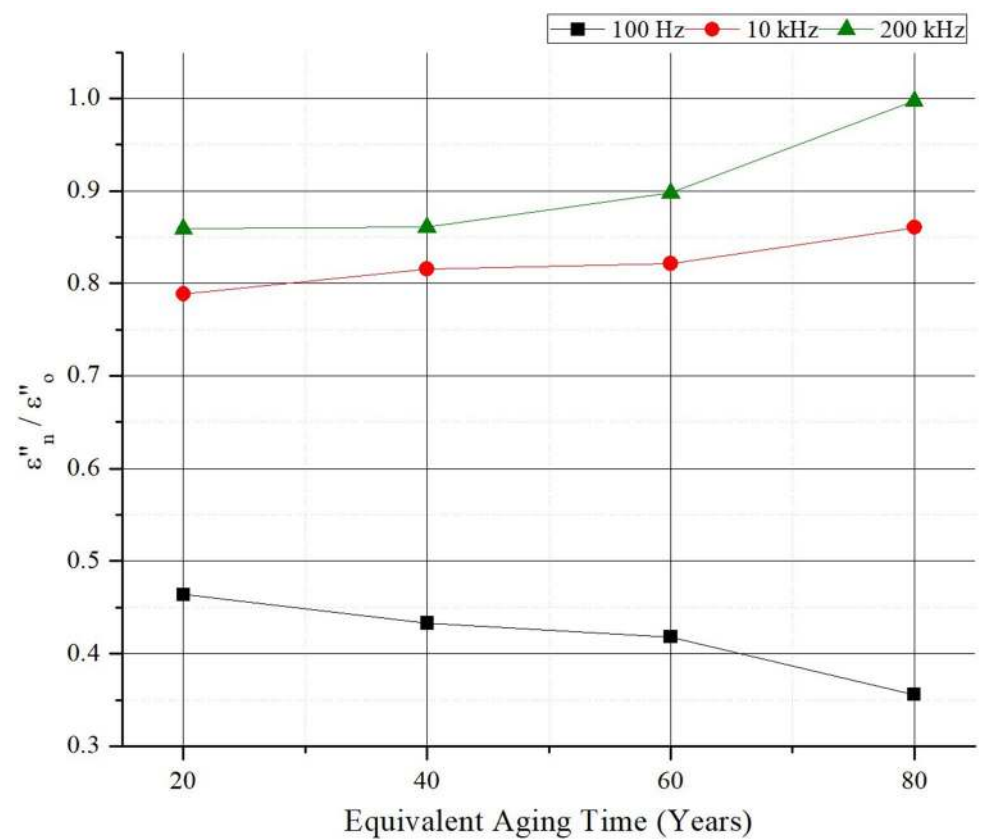
Fig. 9 The behavior of tanδ at 100 Hz, 200 Hz, and 400 Hz vs. Equivalent Aging Time in Years with reference to unaged values

the hopping of charged particles [33]. This creates a low energy field for the electrode charges to occupy these sites, resulting in the increase of the specific conductivity of the material, since S_d is measured when the electrode charges are discharged inside the material after disconnecting from the voltage source [34].

The results of the S_r as a function of the discharging time, Fig. 7, suggests the validity of the results of the dielectric analysis in terms of diagnostic purposes. Since the long discharging time plot helps in estimating the presence of slow polarization processes such as bulk, interfacial and hopping polarizations. Meanwhile, in our case the insulation and jacket are intact so the interfacial and bulk polarizations are more under consideration then the hopping polarization. The initial increase in the S_r values shows that due to the structural changes happening inside the matrix results in increasing the polarization stress on the interface of the jacket and insulation. While the decrease in the values of S_r after the third and fourth thermal cycles were due to the chemical species interaction at high thermal stress, resulting in a reduction in the interfacial polarization. This is understandable as with more thermal stress, it is easy for the chemical species to interact and thus resulting in a decrease in the polarization and amount of aging.

The phenomenon of the re-creation of cross-linking, which is observed in semi-crystalline materials due to

exposure for a long time at elevated temperature results in the decrease in the values of the ε'', tanδ, and S_r.

5 Conclusions

In this work, the effect of thermal stress on the XLPO based LV PV DC cables were analyzed. With component analyzer, the real (ε') and imaginary part (ε'') of permittivity and tanδ for a wide range of frequency were measured and with the EVR, decay voltage (S_d) and return voltage (S_r) slopes were analyzed. It was observed that with the effect of thermal stress, the polymer matrix was altered and the species contributing to the conduction and polarization phenomenon were reduced with aging.

The results of ε'', tanδ and S_r show that the thermally-induced changes in XLPO were because of re-cross-linking reactions; as observable by the noticeable decrease in the values, a phenomenon associated with semi-crystalline materials when exposed to high temperatures. This resulted in a decrease in the interfacial and bulk polarization processes inside the material with the aging time. The tanδ at 100 Hz, the ε'' at 100 Hz and the S_r showed good results of the state of the cable insulation, hence making them feasible to use as electrical aging markers for the assessement of the cable insulation condition. It can be speculated that these methods being non-destructive and simple can be used as

diagnostic techniques effectively with the potential of being applied in the field for the online monitoring of the condition of the cables for the PV system, which is important for its reliability and safe operation. Also, this research work can be helpful in scaling-up the current cable qualification standard. For the future perspective, setting the threshold values of the aging markers the prediction of the remaining life of the PV cable can be evaluated in addition to the determination of the state of the cable.

References

1. E. Mustafa, R. S. A. Afia, Z. Á. Tamus, *Lecture Notes in Electrical Engineering*, ed. by B. Németh (Springer, Cham, 2020)
2. A. Jäger-Waldau, Energies (2019). https://doi.org/10.3390/en12050769
3. International Renewable Energy Agency IRENA, Abu Dhabi, UAE (2018)
4. K. Vyas, *Managing Solar Cables and Connectors For Safety and Longevity of PV System* (New Delhi, India, 2017)
5. F. Schimpf, L. E. Norum, In 31st Int. Telecommun. Energy Conf., Incheon, Korea, (2009)
6. J. Packa, V. Kujan, D. Štrkula, V. Šály, M. Perný, Trans. Electr. Eng. **6**, 6–9 (2017). https://doi.org/10.14311/TEE.2017.1.006
7. K. Padmanathan, U. Govindarajan, V.K. Ramachandaramurthy, S.O. Selvi, B. Jeevarathinam, J. Ind. Inf. Integr. (2018). https://doi.org/10.1016/j.jii.2018.01.003
8. G. Parise, L. Martirano, IEEE Trans. Ind. Appl. **50**(3), 2156–2163 (2014). https://doi.org/10.1109/TIA.2013.2283197
9. Z. Zhang, P.D.S. Assala, L. Wu, Electr. Power Syst. Res. **163**, 572–580 (2018). https://doi.org/10.1016/j.epsr.2017.12.027
10. M. Celina, K.T. Gillen, J. Wise, R.L. Clough, Radiat. Phys. Chem. **48**, 613–626 (1996). https://doi.org/10.1016/0969-806X(96)00083-7
11. A. Paramane, X. Chen, C. Dai, H. Guan, L. Yu, Y. Tanaka, Polym. Compos. (2020). https://doi.org/10.1002/pc.25509
12. International Atomic Energy Agency, *IAEA* (Austria, Vienna, 2017)
13. M. Celina, K. T. Gillen, R. L. Clough, *Annealing Phenomena in the Radiation Degradation of Crosslinked Polyolefins* (IAEA-TECDOC--1062), International Atomic Energy Agency (IAEA), (1999)
14. M. Celina, K.T. Gillen, R.L. Clough, Polym. Degrad. Stab. **61**, 231–244 (1998). https://doi.org/10.1016/S0141-3910(97)00142-0
15. E. Mustafa, R. S. A. Afia, Z. Á. Tamus, In: 7th Int. Youth Conf. Energy, Bled, Slovenia (2019)
16. Z. Zhou, D. Zhang, J. He, M. Li, I.E.E.E. Trans, Dielectr. Electr. Insul. **22**, 2097–2107 (2015). https://doi.org/10.1109/TDEI.2015.004799
17. M. Ekelund, P.F. Fantoni, U.W. Gedde, Polym. Test **30**, 86–93 (2011). https://doi.org/10.1016/j.polymertesting.2010.11.003
18. L. Verardi, D. Fabiani, G.C. Montanari, Radiat. Phys. Chem. **94**, 166–170 (2014). https://doi.org/10.1016/j.radphyschem.2013.05.038
19. N. Bowler, S. Liu, Progn. Heal. Manag. Soc. pp. 1–12 (2015) https://www.phmsociety.org/node/1638
20. S.Z.A. Dabbak, H.A. Illias, B.C. Ang, N.A.A. Latiff, M.Z.H. Makmud, Energies (2018). https://doi.org/10.3390/en11061448
21. N. Bashir, H. Ahmad, M. Shaffuan Suddin, In: IEEE 2010 Conf. Proc. IPEC., Singapore, Singapore, pp. 1062–1066 (2010)
22. C. D. Paraskevas, P. Vassiliou, C. T. Dervos, In: IEEE Int. Conf. Dielectr. Liq., Coimbra, Portugal, pp. 275–278 (2005)
23. S.Z. Dabbak, H.A. Illias, B.C. Ang, I.E.E.E. Trans, Dielectr. Electr. Insul. **24**, 3758–3765 (2017). https://doi.org/10.1109/TDEI.2017.006418
24. E. Barsoukov, J.R. Macdonald, *Impedance Spectroscopy Theory, Experiment, and Applications* (Wiley, New Jersey, 2010)
25. M. Farahani, H. Borsi, E. Gockenbach, Electr. Eng. **89**, 263–270 (2007). https://doi.org/10.1007/s00202-006-0011-9
26. E. Mustafa, Á. Z. Tamus, R. S. A. Afia, *IFIP Advances in Information and Communication Technology*, ed. by L. Camarinha-Matos, R. Almeida, J. Oliveira (Springer, Cham, 2019), p. 405 https://doi.org/10.1007/978-3-030-17771-3_35
27. E. Mustafa, R.S.A. Afia, Á.Z. Tamus, In: 2018 Int. Conf. Diagn. Electr. Eng, Pilsen, Czech Republic, pp. 69–72 (2018)
28. Z. Á. Tamus, G. M. Csányi, Á. Szirmai, A. Nagy, In: Int. Sci. Symp. Electr. Power Eng., Varna, Bulgaria, pp. 7–13 (2016)
29. G. M. Csányi, Z. Á. Tamus, In: 2017 6th Int. Youth Conf. Energy, Budapest, Hungary, pp. 2–5 (2017) https://doi.org/10.1109/IYCE.2017.8003702
30. Á. Z. Tamus, Á. Szirmai, B. Németh, In: The 19th Int. Symp. High Volt. Eng., Pilsen, Czech Republic (2015)
31. E. Nemeth, IEE Proc- Sci. Meas. Technol. **146**(5), 249–252 (1999). https://doi.org/10.1049/ip-smt:19990651
32. X. Chen, A. Paramane, H. Liu, J. Tie, Z. Wei, Y. Tanaka, Polym. Eng. Sci. (2020). https://doi.org/10.1002/pen.25330
33. S. Morsalin, T.B. Phung, M. Danikas, D. Mawad, IET Sci. Meas. Technol. **13**(6), 767–782 (2019). https://doi.org/10.1049/iet-smt.2018.5597
34. D. Min, C. Yan, Y. Huang, S. Li, Y. Ohki, Polym. (Basel) **9**, 1–15 (2017). https://doi.org/10.3390/polym9100533